

# Passive Microwave Remote Sensing of the Ocean: an Overview

Chelle L. Gentemann, Frank J. Wentz, Marty Brewer, Kyle Hilburn, and Deborah Smith

Remote Sensing Systems, Santa Rosa, CA, USA

**Abstract.** Passive microwave observations from satellites provide measurements of sea surface temperature (SST), wind speed, water vapor, cloud liquid water, rain rate, and sea ice that have led to significant advances in meteorological and oceanographic research as well as improvements in monitoring and forecasting both weather and climate. Future instruments are planned to measure sea surface salinity. The calibration of passive microwave radiometers has continued to improve, along with the retrieval algorithms. The production of accurate geophysical retrievals depends on the close development of both calibrated brightness temperatures and retrieval algorithm design in concert. Data must be carefully screened for near-land emissions, radio frequency interference, rain scattering (for SST, wind, and vapor retrievals), and high wind events (SST retrievals only).

## 1. Introduction

Global geophysical measurements from passive microwave radiometers provide key variables for scientists and forecasters. The daily measurements of Sea Surface Temperature (SST), wind speed, water vapor, cloud liquid water, rain rate, and, in the future, Sea Surface Salinity (SSS) over the oceans has provided data sets used to significantly improve our understanding of the Earth system. The data are used extensively in numerical weather prediction, hurricane forecasting, climate monitoring, ecosystem forecasting and fisheries; as well as for climate, weather, oceanographic, meteorological and ecosystem research. The measurement accuracy is tied to the evolution of both the calibration methods and retrieval algorithms.

## 2. Background

Designed to measure rainfall, the first Passive MicroWave (PMW) radiometer was launched in December 1972 on the Nimbus-5 satellite. After a

short gap, PMW radiometers have been continuously observing the oceans since the launch of Nimbus-7 in 1978. This instrument was followed by the Special Sensing Microwave Imager (SSM/I) series. More recently, several other PMW radiometers have been launched on National Aeronautics and Space Administration (NASA), Japan Aerospace eXploration Agency (JAXA), and European Space Agency (ESA) satellites (Table 1).

**Table 1.** PMW radiometer mission characteristics

Satellite	Sensor	Launch	Failure	Frequency (GHz)	Coverage
Nimbus-5	ESMR	12/1972	5/1977	19.4	Global
Nimbus-7	SMMR	10/1978	8/1987	6.6, 10.7, 18.0, 21.0, 37.0	Global
SEASAT	SMMR	6/1978	10/1978	6.6, 10.7, 18.0, 21.0, 37.0	Global
DMSP F08	SSM/I	7/1987	12/1991	19.4, 22.2, 37.0, 85.5	Global
DMSP F10	SSM/I	12/1990	11/1997	19.4, 22.2, 37.0, 85.5	Global
DMSP F11	SSM/I	12/1991	5/2000	19.4, 22.2, 37.0, 85.5	Global
DMSP F13	SSM/I	5/1995	Present	19.4, 22.2, 37.0, 85.5	Global
DMSP F14	SSM/I	5/1997	8/2008	19.4, 22.2, 37.0, 85.5	Global
DMSP F15	SSM/I	12/1999	Present	19.4, 22.2, 37.0, 85.5	Global
TRMM	TMI	12/1997	Present	10.7, 19.4, 21.3, 37.0, 85.5	40S-40N
ADEOS-II	AMSR	12/2002	10/2003	6.9, 10.7, 18.7, 23.8, 36.5, 89.0	Global
AQUA	AMSR-E	5/2002	Present	6.9, 10.7, 18.7, 23.8, 36.5, 89.0	Global
Coriolis	WindSat	6/2003	Present	6.8, 10.7, 18.7, 23.8, 37.0	Global
DMSP F16	SSM/I/S	10/2003	Present	-	Global
DMSP F17	SSM/I/S	11/2006	Present	-	Global
SMOS	MIRAS	11/2009	-	1.4	Global
GPM	GMI	(7/2013)	-	10.7, 18.7, 23.8, 36.5, 89.0	65S-65N
SAC-D	Aquarius	(5/2010)	-	1.4	Global
GCOM-W	AMSR2	(2/2012)	-	6.9, 7.3, 10.7, 18.7, 23.8, 36.5, 89.0	Global
C2	MIS	(5/2016)	-	6.8, 10.7, 18.7, 23.8, 37.0, 89.0	Global

The Electrically Scanning Microwave Radiometer (ESMR) on Nimbus-5 had only one channel at 19.35 GHz and was capable of measuring both rainfall and sea ice detection.

From October 1978 through July 1987, the Nimbus-7 Scanning Multi-channel Microwave Radiometer (SMMR) measured at 6.6, 10.7, 18.0, 21.0, and 37 GHz in both the horizontal and vertical polarizations (Gloersen *et al.*, 1984). SMMR geophysical retrievals were compromised by non-negligible switch leakages (Han and Kim, 1988), rendering the

SMMR measurements useful for detection of sea ice but not accurate enough for geophysical retrievals.

The Defense Meteorological Satellite Program (DMSP) satellite series launched the first SSM/I on F-08 in June 1987. This was followed by SSM/Is on F-09 through F-15. The DMSP satellites orbit the earth in 102 minutes, at approximately 833 km with an inclination of  $98.8^\circ$  (Hollinger *et al.*, 1990). The F-series alternate between early and late morning Local Equator Crossing Times (LECTs). The SSM/I instrument measures at 19.4, 22.2, 37.0, and 85.5 GHz. Both vertical and horizontal polarizations are measured for all channels except the 22.2 GHz which only measures the vertical. SSM/I was the first satellite PMW radiometer to have external calibration accomplished by viewing a mirror that reflects cold space and a hot reference absorber once each scan, every 1.9 seconds. The cold space is a known 2.7 K while the hot absorber temperature is monitored with thermistors. The frequent calibration minimizes receiver gain fluctuation contributions to the signal but does not correct radiometer nonlinearity (if it exists). This well-calibrated instrument's measurements are used to determine wind speed, water vapor, cloud liquid water, rain rates, and sea ice concentration over global oceans.

In December 1997, NASA launched the Tropical Rainfall Measuring Mission (TRMM) carrying the TRMM Microwave Imager (TMI), a PMW radiometer measuring at 10.7, 19.4, 21.3, 37.0, and 85.5 GHz. Similar to SSM/I, all channels measure both vertical and horizontal polarizations, except the 21.3 GHz which only measures in the vertical (Kummerow *et al.*, 1998). Designed to measure the tropics and sample the diurnal cycle, the satellite was launched with an orbital inclination of  $35^\circ$  at an altitude of 350 km (later changed to 400 km to extend satellite life). This equatorial orbit yields coverage from 39N to 39S. The satellite is sun-asynchronous, processing through the diurnal cycle every 23 days. Again, similar to SSM/I, the feed horns and main reflector rotate, with a period of 1.9 seconds, about an axis parallel to the local spacecraft nadir. The stationary hot reference absorber and cold calibration reflector are positioned so that they pass between the feed horns and main reflector once per scan. The temperature of the warm load is monitored by three thermistors while the cold reflector views the cosmic microwave (MW) background at 2.7 K. At fairly regular intervals the platform yaws from forward (aft) viewing direction to aft (forward). Each scan consists of 104 discrete samples spaced by 8 km. In addition to the geophysical variables measured by SSM/I, TMI is able to measure SST. TMI suffered calibration problems due to an emissive reflector, for which corrections were developed and implemented.

NASA's AQUA satellite carries the JAXA's Advanced Microwave Scanning Radiometer - Earth Observing System (AMSR-E). The AQUA

satellite was launched in May 2002 into a polar, sun-synchronous orbit at an altitude of 705 km, with a LECT of 1:30 AM/PM. AMSR-E has 12 channels corresponding to 6 frequencies: 6.9, 10.7, 18.7, 23.8, 36.5, and 89.0 GHz, all except 23.8 measure both vertical and horizontal polarizations (Parkinson, 2003). The calibration is completed similar to SSM/I and TMI using a cold reflector and hot absorber with 8 thermistors. The AMSR-E hot absorber has large thermal gradients not well measured by the thermistors. A correction for this error in the calibration reference point has been developed and implemented. In addition to the geophysical variables measured by SSM/I, AMSR-E is able to measure SSTs. Almost global coverage is attainable in 2 days (Figure 1).

The Naval Research Laboratory (NRL) launched the Coriolis satellite in January 2003. The sun-synchronous orbit is at an altitude of 840 km with a LECT at 6:00 AM/PM (Gaiser *et al.*, 2004). Coriolis carries the Wind-Sat instrument, a fully polarimetric PMW radiometer intended to retrieve wind direction in addition to wind speed. The fully polarimetric channels are at 10.7, 18.7, and 37.0 GHz, but the instrument also has channels at 6.8 and 23.8 that only measure the vertical and horizontal polarizations. Calibration is similar to SSM/I with a cold reflector and hot absorber measured by 6 thermistors.

DMSP satellites F16 and forward carry the Special Sensor Microwave Imager/Sounder (SSMIS). F16 was launched in October 2003 into a sun-synchronous orbit at an altitude of 830 km and a LECT of 8 AM/PM. SSMIS has 24 channels, several of which are similar to the SSM/I set (19.35, 22.2, and 37.0 GHz). The additional channels are intended for atmospheric sounding. The calibration is completed similar to SSM/I using a cold reflector and hot absorber. SSMIS has two main problems, an emissive antenna and non-uniform hot absorber. Corrections for these issues have been developed and implemented.

Future PMW radiometers include JAXA's Global Change Observation Mission – Water (GCOM-W) AMSR2, the National Polar Orbiting Earth observing System of Systems (NPOESS) C2 satellite will carry the Microwave Imager Sounder (MIS), and NASA's Global Precipitation Mission (GPM) will carry the GPM Microwave Imager (GMI). For all these instruments, the planned calibration is similar to SSM/I using a cold reflector and hot absorber.

GCOM-W is to be launched in February 2012 into NASA's A-Train satellite formation in a sun-synchronous orbit with an altitude of 700 km and a LECT of 1:30 AM/PM. AMSR2 is similar to AMSR-E but has an improved hot absorber and an additional channel at 7.3 GHz to minimize Radio Frequency Interference (RFI). With a launch date set for February

2012, it is hoped that the AQUA AMSR-E remains healthy until then to allow for satellite inter-calibration.

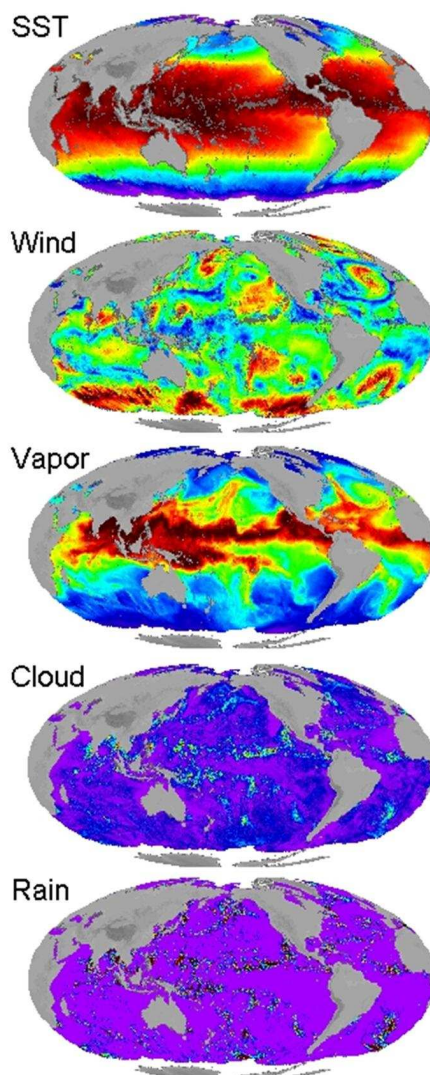


**Fig. 1.** AMSR-E geophysical retrievals 1-2 October 2009. Small amounts of missing data due to rain events are visible in the SST and wind retrievals.

Two other future instruments, the European Space Agency's Soil Moisture and Ocean Salinity (SMOS) Microwave Imaging Radiometer using Aperture Synthesis (MIRAS) and the Satélite de Aplicaciones Científicas-

D (SAC-D) Aquarius are intended to measure ocean salinity and only have a single channel at 1.4 GHz. SMOS launched in November 2009 into a sun-synchronous orbit at 800 km with an LECT of 6:00 AM/PM. Aquarius is scheduled to be launched in May 2010 into a sun-synchronous orbit at 650 km with a LECT of 6:00 AM/PM. Both of these instruments are designed to provide measurements of ocean salinity.

### 3. Calibration

To create a climate quality, inter-calibrated dataset of PMW geophysical retrievals, it is necessary to start the process using radiometer counts and work towards calibrated geophysical retrievals. Table 2 describes the steps to produce a calibrated brightness temperature (TB). First, it is necessary to reverse engineer the antenna temperatures (TAs) or TBs back to radiometer counts. Often there are small provider added corrections or adjustments put into the TA or TBs which are sometimes undocumented. For example, SSMI/S had five TB version changes in the first two years of data. Therefore, the first step is to reverse these steps and remove any corrections. Starting from radiometer counts, the first two steps in the calibration procedure are crucial to accurately determining other errors.

**Table 2.** Calibration steps for PMW radiometers

	Geolocation analysis	Attitude adjustment	Along-scan correction	Absolute calibration	Hot load correction	Antenna emissivity
SSM/I	NRL/RSS	No	Yes	APC	No <sup>1</sup>	0
TMI	Goddard	Dynamic	Yes	APC	No	3.5%
AMSRE	RSS	Fixed	Yes	APC	Yes	0
AMSRA	RSS	Dynamic	Yes	APC	Yes	0
WindSat	NRL/RSS	Fixed	Yes	APC	Yes	0
SSMIS	RSS	No	Yes	APC	Yes	0.5-3.5%

To ensure that any subsequent collocations or comparisons that are performed are correct, it is necessary to do a geolocation analysis. The correction to the geolocation is different than a correction for erroneous satellite pointing information (roll/pitch/yaw). This is a correction for the mounting of the instrument on the satellite. Pointing is usually off by

<sup>1</sup> Errors due to hot load are removed when doing the zonal TB inter-calibration

about  $0.1^\circ$  from the satellite specified roll/pitch/yaw. The geolocation correction uses ascending minus descending TA to ensure that islands do not 'move'. The geolocation analysis has been performed by a number of groups, NRL and Remote Sensing Systems (RSS) both contributed to SSM/I, TMI was completed by Goddard, and other instruments as specified in Table 2.

Corrections from this point onward are determined by comparisons between the satellite TA measurements and TAs simulated using a radiative transfer model (RTM). Using collocated environmental information, RTM simulated TBs are determined. These TBs are then transformed into TAs using the instrument, channel specific antenna patterns.

After the pointing is corrected, the spacecraft reported roll/pitch/yaw are then examined for errors using comparisons of the observed minus RTM TAs. Spacecraft pointing is determined by a number of different methods, the preferred being a star tracker. Another method is horizon balancing sensor. For SSM/I no pointing information was given, so it was assumed to be correct. TMI has a dynamic pointing correction that changes within an orbit because the horizon sensor used prior to the orbit boost is not as accurate as a star tracker. After boost, the horizon sensor was disabled and pointing was determined from two on-board gyroscopes, also not as accurate as a star tracker. AMSR-E had no pointing problems, as the AQUA had a star tracker. The AMSR on ADEOS-II needed a dynamic correction, while WindSAT needed a simple fixed correction to the roll/pitch/yaw.

Once instrument mounting errors and satellite attitude errors have been corrected for, an along-scan correction is completed. It is very important to complete the first two corrections first because TA is dependent on incidence angle. Not correcting for pointing errors would result in an erroneous cross-scan biasing. As the mirror rotates, at the edge of the earth scene the view will begin to contain obstructions such as the satellite itself or part of the cold mirror. Additionally, during the scan, the antenna side-lobe pattern may result in contributions from different parts of the spacecraft. Therefore the difference between the TA and RTM simulated TAs are again used to examine the data for along-scan biases. This correction is needed for every instrument.

The antenna pattern correction (APC) is then completed. Pre-launch, an APC is determined, consisting of the spill over and cross-polarization values. After launch the spill over and cross-polarization values are adjusted so that the measured TAs matches the simulated TAs. This correction is needed for all instruments. Next, a correction for the hot load thermal gradients and antenna emissivity are developed. These are only needed for specific instruments. The determination of TB from counts for PMW radiometers is completed using two known temperatures to infer the scene

temperature. For each scan, the feedhorns view a mirror that reflects cold space, a known 2.7 K, a hot absorber, measured by several thermistors, and Earth scenes. Assuming a linear response, the Earth scene temperatures are then determined by fitting a slope to the two known measurements as shown in Figure 2. This 2-point calibration system continuously compensates for variations in the radiometer gain and noise temperatures. This seemingly simple calibration methodology is fraught with subtle difficulties. The cold mirror is relatively trouble-free, as long as lunar contamination is flagged. Occasionally, the cold mirror will not reflect deep space, but the moon instead. These data must be removed.

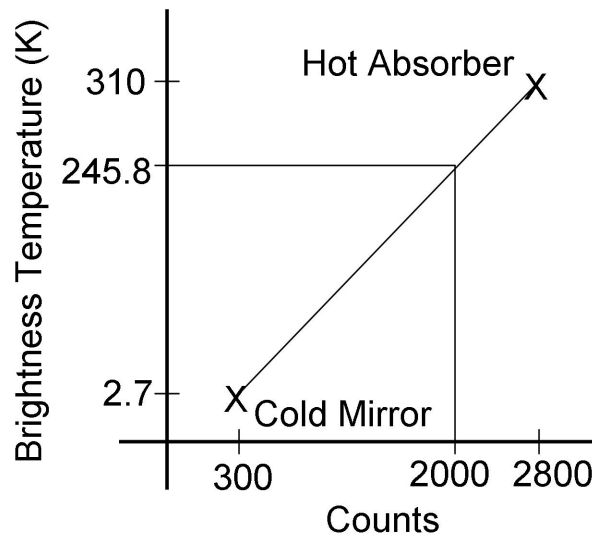


**Fig. 2.** Calculation of Earth scene brightness temperatures using the radiometer counts and calibration points (cold mirror and hot absorber) known temperatures.

The hot absorber has been more problematic as the thermistors often do not adequately measure thermal gradients across the hot absorber. For example, a hot load correction is required for AMSR-E because of a design flaw in the AMSR-E hot load. The hot reference load acts as a blackbody emitter and its temperature is measured by precision thermistors. Unfortunately, during the course of an orbit, large thermal gradients develop within the hot load due to solar heating making it difficult to determine the average effective temperature from the thermistor readings. The thermistors themselves measure these gradients and may vary by up to 15 K between themselves at any time for AMSR-E. Several other instruments have had similar, but smaller, issues. RTM simulations are used to deter-

mine an effective hot load temperature which is a regression of the measured hot load thermistor temperatures. The follow-on instrument, AMSR2 on GCOM-W, has an improved hot absorber design that should mitigate these issues.

Finally, the main reflector is assumed to be a perfect reflector with an emissivity of 0.0, but this is not always the case. For example, a bias recognized in the TMI measurements was attributed to the degradation of the primary antenna. Atomic oxygen present at TMI's low altitude (350 km) led to rapid oxidization of the thin, vapor-deposited aluminum coating on the graphite primary antenna, resulting in a much higher antenna emissivity than expected. The measured radiation is comprised of the reflected earth scene and antenna emissions. Emissivity of the antenna was deduced during the calibration procedure to be 3.5%. The antenna emissivity correction utilizes additional information from instrument thermistors to estimate the antenna temperature, thereby reducing the effect of the temporal variance. This emissivity is constant for all the TMI channels. SSMI/S has an emissive antenna where the emissivity appears to increase as a function of frequency, changing from 0.5 – 3.5 %.

#### **4. Retrieval algorithm**

Geophysical retrievals from PMW radiometers are commonly determined using a radiative transfer model to derive a regression algorithm (Wentz, 1998). A schematic of the derivation of the regression coefficients is shown in Figure 3. A large ensemble of ocean-atmosphere scenes is first assembled. The specification of the atmospheres comes from quality-controlled radiosonde flights launched from small islands (Wentz, 1997). One half of these radiosonde flights are used for deriving the regression coefficients, and the other half is withheld for testing the algorithm. A cloud layer of various columnar water densities ranging from 0 to 0.3 mm is superimposed on the radiosonde profiles. Underneath these simulated atmospheres, we place a rough ocean surface. SST is randomly varied from 0 to 30 °C, the wind speed is randomly varied from 0 to 20 ms<sup>-1</sup>, and the wind direction is randomly varied from 0 to 360°.

Atmospheric brightness temperatures and transmittance are computed from these scenes and noise, commensurate with measurement error which depends on spatial resolution, is added. The noise-added simulated brightness temperatures along with the known environmental scene are used to generate multiple linear regression coefficients. Algorithm testing is undertaken by repeating the process using the withheld scenes.

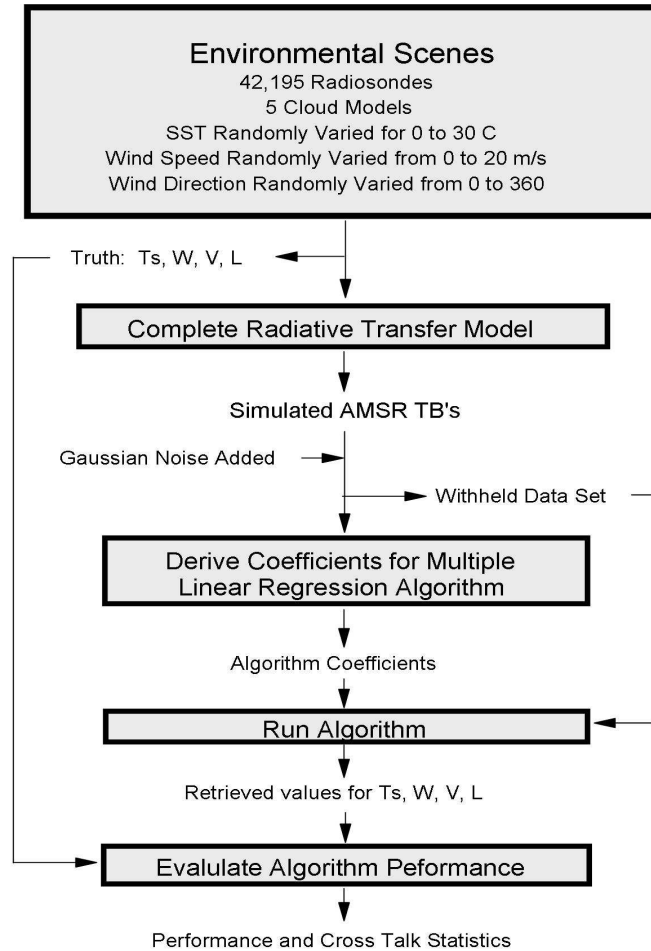


**Fig. 3.** Derivation of regression coefficients

## 5. Geophysical retrievals

### Wind speed

Ocean surface winds are crucial to transferring heat, gases, energy and momentum between the atmosphere and ocean. Winds also determine the large scale ocean circulation and transport, power global weather patterns, and play a key role in marine ecosystems. Hurricanes, typhoons, and mid-latitude winter storms all contain high wind speeds that threaten international shipping and the lives and property of people along the coasts.

Ocean surface winds change rapidly in both time and space and satellite sampling and accuracy make these observations the most useful wind data available for research and forecasting over the global oceans.

Surface wind speeds (at 10 m height, without directions) are routinely estimated from passive microwave radiometers (SSM/I, AMSR-E, TMI, SSMIS) on a spatial scale of roughly 25 km. Wind speeds in the range of 0 to 30  $\text{ms}^{-1}$  are simultaneously retrieved along with SST, water vapor, cloud liquid water and rain rates using an algorithm that exploits the polarization signature of wind induced sea surface emissivity (Wentz, 1997). Radiometer winds are quite accurate under typical ocean conditions when no rain is present, however when even a little rain exists, the wind speeds are unusable. Validations of radiometer winds in rain-free conditions have been performed. Comparisons with ocean buoy and weather model winds show root-mean-square differences near (model winds) or less than 1  $\text{ms}^{-1}$  (buoy winds) in rain-free conditions (Mears *et al.*, 2001; Meissner *et al.*, 2001). Since 1996, there have been three or more radiometers in polar orbits simultaneously, resulting in good spatial and temporal sampling, yielding over 95% Earth ocean surface coverage in a given day.

WindSat is a passive fully-polarimetric microwave radiometer designed to measure ocean surface vector winds. It has been found to have wind accuracies close to that of scatterometers for winds between 6 and 20  $\text{ms}^{-1}$ , with significant wind direction uncertainty below 6  $\text{ms}^{-1}$  (Bettenhausen *et al.*, 2006). WindSat vector winds have been poor in rainy conditions until recently when a new WindSat algorithm has been developed that improves WindSat winds even in rain (Meissner and Wentz, 2009). The quality of these new winds is similar to QuikScat in all but very heavy rain and very low winds. Excellent agreement (to within 0.5  $\text{ms}^{-1}$ ) is found between passive radiometer wind speeds, polarimetric radiometer wind vectors and scatterometer vector winds despite the different measuring methods of each instrument (Wentz and Meissner, 2007). Only a few small regions of difference exist that seem to be related to the 37 GHz observations of the ocean surface and atmosphere.

Combined surface wind data sets have recently become more available and are very useful in atmospheric and oceanographic research due to the lack of data gaps. One example, the Cross Correlated Multi-Platform (CCMP) winds (Atlas *et al.*, 2009), use carefully inter-calibrated PMW wind speeds from radiometers and wind vectors from scatterometers. Simple interpolation schemes are unable to adequately represent fast-moving storms in mid-latitude regions when making a merged wind product with no gaps. An advanced 4-dimensional variational analysis method is used in the CCMP to merge the satellite winds with the European Center for Medium-range Weather Forecasting (ECMWF) Re-Analysis (ERA)-40

model wind vectors, providing a gridded wind product consisting of an analyzed wind field every six hours for 20 years.

The satellite winds used in the CCMP include over 20 years of SSM/I winds. A recent study showed that these carefully inter-calibrated SSM/I winds have no spurious trends. Wentz *et al.* (2007) found agreement between ocean buoy trends and the SSM/I trends for many buoy types and different ocean regions. The overall difference in wind trend (SSM/I minus buoy) is  $-0.02 \text{ ms}^{-1}/\text{decade}$ . This gives one confidence in using the passive microwave winds in climate studies.

### **Water Vapor**

Over 99% of the atmospheric moisture is in the form of water vapor, and this vapor is the principal source of the atmospheric energy that drives the development of weather systems on short time scales and influences the climate on longer time scales. Tropospheric water vapor measurements are an important component to the hydrological cycle and global warming (Held and Soden, 2006; Trenberth *et al.*, 2005). The microwave measurement of water vapor can also be used as a proxy to detect global warming of the lower troposphere with a signal-to-noise ratio that is five times better than the AMSU method of measuring the temperature change (Wentz and Schabel, 2000).

Satellite microwave measurements near the 22.2 GHz vapor absorption line provide the most accurate means to determine the total amount of vapor in the atmosphere. Quality controlled radiosondes from stations on small islands or ships are used for validation of the columnar water vapor retrievals. Simulations show that retrievals are accurate to 0.1 mm total columnar water vapor. Comparisons of AMSR-E water vapor retrievals with ship based radiosondes show an error of 2.2 - 0.5 mm (Szczo drak *et al.*, 2006) which includes errors due to differences between a radiosonde point measurement and the larger AMSR-E footprint.

### **Cloud Liquid Water**

Cloud water links the hydrological and radiative components of the climate system. Cloud water can be retrieved from passive microwave measurements because of its strong spectral signature and polarization signature (Wentz, 1997). Passive microwave observations provide a direct estimate of the total absorption along the sensor viewing path. At 18 and 37 GHz, clouds are semi-transparent allowing for measurement of the total columnar absorption. The absorption is related to the total amount of liq-

uid water in the viewing path, after accounting for oxygen and water vapor absorption.

Validation of columnar cloud liquid water is a difficult undertaking. The spatial variability of clouds makes comparisons between upward looking ground based radiometers and the large footprint size of the downward looking satellite retrievals problematic. The upward looking ground-based radiometers also have very limited geographic distribution, making meaningful validation over global conditions impossible. Generally, validation is completed using a statistical histogram method (Wentz, 1997).

### **Rain Rate**

Rainfall is the key hydrological parameter, so much so that changes in the spatial distribution of rainfall have led to the collapse of civilizations (Haug *et al.*, 2003; O'Conner and Kiker, 2004). Rain is one of the most difficult parameters to accurately retrieve using remote sensing because of its extreme variability in space and time over a variety of scales. The most accurate and physically-based rain retrieval techniques take advantage of the interactions between microwave radiation and water, and both passive and active microwave remote sensing techniques can be used to derive rain rates over both ocean and land.

PMW observations respond to the presence of rain in the instrument field-of-view with two primary signals: an emission signal and a scattering signal (Petty, 1994). The ocean surface is roughly 50% emissive, so it serves as a cold background around 150 K against which to observe rain. Since the ocean is an expansive flat surface, the emission is strongly polarized. For typical incidence angles and clear skies, vertical polarization brightness temperatures are larger than horizontal polarization brightness temperatures by as much as 100 K. The emission depends on the sea surface temperature, salinity, and surface roughness.

Emission from small round rain and cloud drops is unpolarized, and the liquid emission strongly decreases the polarization seen by the sensor. Heavy rain can bring the difference between vertical and horizontal polarization brightness temperatures down to zero. The emission signal has a strong spectral signature that increases with frequency – that is, higher microwave frequencies are more affected by rain. The strength of the emission signal depends on the total amount of liquid water below the freezing level, and this is related to the surface rain rate. The primary factors governing this relationship are: the height of the freezing level, the relative portioning of cloud and rain water, and the effect horizontal inhomogeneity – the beamfilling effect (Hilburn and Wentz, 2008; Wentz and Spencer, 1998). The scattering signal measures a decrease in brightness tempera-

tures due to the presence of ice above the freezing level (Spencer *et al.*, 1989). Usually the scattering signal is used over a warm background, and is especially useful over land. The relationship of the scattering signal to surface rain rate is less direct than it is for the emission signal.

The relationship between the emission signal and the rain rate is strongly nonlinear. Since rain is horizontally inhomogeneous over satellite footprints (which may range in diameter from 6 - 56 km), the measurement represents an average over the satellite footprint. Averaging a highly variable observable quantity, when the observable quantity is nonlinearly related to the desired quantity, results in a bias in the desired quantity. This is the beamfilling effect, and it causes rain rates to be underestimated by PMW radiances.

Different sensors have systematically different spatial resolutions and the probability distribution function of liquid water in the footprint changes systematically with the size of the footprint. For example, an infinitely small satellite footprint would model the variability of liquid in the footprint with a delta function, whereas a satellite footprint the size of the Earth models that variability with the global rain probability distribution function – typically taken to be a mixed log-normal distribution. Fortunately, real satellite footprints do not vary that much. The spatial resolution of SSM/I rain retrievals is nominally 32 km, and the spatial resolution of AMSR rain retrievals is nominally 12 km. This means that SSM/I rain retrievals require a larger beamfilling correction than AMSR rain retrievals, because SSM/I retrievals have more spatial averaging.

(Hilburn and Wentz, 2008) developed a new beamfilling correction by simulating lower resolution SSM/I data with higher resolution AMSR data. Rain retrievals were computed from the simulated SSM/I data at several resolutions and compared to the AMSR rain retrievals at the highest possible resolution to deduce how the variability of liquid water changes systematically with footprint size. When the new correction was applied to satellite data, rain rates agreed to within 3% (after removing sampling biases due to the different local times-of-day for each satellite). New intercalibrated rain rate retrievals have been successfully used to close the water cycle (Wentz *et al.*, 2007), show excellent agreement with rain gauges on ocean buoys (Bowman *et al.*, 2009), and correlate well with the TRMM Precipitation Radar (Cecil and Wingo, 2009).

## Sea Ice

PMW retrievals of sea ice form one of the most important climate data records in existence. The time series of sea ice, from 1979 – present, has provided measurements of ice concentration and classification of sea ice

types (multiyear or first-year ice) on a daily basis. The PMW sea ice retrievals are vital because of their ability to see through clouds. Large ice shelf breakup events, such as the Larsen Ice shelf breakup, have been witnessed and monitored using PMW retrievals. Sea ice is important to the global climate as it acts to regulate heat, moisture, and salinity in the polar ocean. The recent increase in summer Arctic sea ice acts as a positive feedback for global warming by changing the albedo.

There are two common retrieval algorithms for sea ice, the NASA team algorithm and the bootstrap algorithm. Both algorithms use the polarization and gradient ratios to determine ice concentration and type. At 19 GHz the difference between the vertical and horizontal polarizations is small for sea ice (both first-year and multiyear) and large for ocean. The two polarizations are different for first-year versus multi-year ice at 37 GHz (Cavalieri *et al.*, 1984). The primary error in the NASA team algorithm is due to the effects of surface glazing and layering on these channel ratios (Comiso *et al.*, 1997). Newer team algorithms use the 89 GHz gradient ratio to minimize these errors (Markus and Cavalieri, 2000). The bootstrap algorithm uses the polarization and gradient ratios, combining different channels, such as the 19 and 37 vertical polarization ratio (Comiso *et al.*, 1997). Both algorithms use different methodologies to filter weather effects.

Validation of the sea ice retrievals has been completed through inter-comparison between different algorithms and comparison to visible and infrared satellite measurements. The NASA team algorithm and bootstrap algorithm generally agree with each other but differ by 10 – 35 % in areas within the ice pack (Comiso and Steffen, 2001).

### **Sea Surface Temperature**

Sea surface temperature is a key climate and weather measurement routinely made each day by satellite infrared (IR) and PMW radiometers, in situ moored and drifting buoys, and ships of opportunity. These measurements are used to create daily spatially-complete global maps of SST that are then used for weather prediction, ocean forecasts, and in coastal applications such as fisheries forecasts, pollution monitoring, and tourism. They are also widely used by oceanography, meteorology, and climate scientists for research. Prior to 1998, SSTs were only available globally from IR satellite retrievals, but with the launch of TMI, PMW retrievals became possible. While IR SSTs have a higher resolution than PMW SSTs (1 – 4 km as compared to 25 km), their retrieval is prevented by clouds giving PMW SSTs improved coverage since they are retrieved through clouds.

Between 4 and 11 GHz the vertically polarized TB of the sea-surface has an appreciable sensitivity to SST. In addition to SST, TB depends on the sea-surface roughness and on the atmospheric temperature and moisture profile. Fortunately, the spectral and polarimetric signatures of the surface-roughness and the atmosphere are quite distinct from the SST signature, and the influence of these effects can be removed given simultaneous measurements at multiple frequencies and polarizations. Both TMI and AMSR-E measure multiple frequencies that are more than sufficient to remove the surface-roughness and atmospheric effects. Sea-surface roughness, which is tightly correlated with the local wind, is usually parameterized in terms of the near-surface wind speed and direction. The additional 7 GHz channel present on AMSR-E and not TMI, provides improved estimates of sea-surface roughness and improved accuracy for SSTs less than 12°C (Gentemann *et al.*, *in press*). All channels are used to simultaneously retrieve SST, wind speed, columnar water vapor, cloud liquid water, and rain rate (Wentz and Meissner, 2000). SST retrieval is prevented only in regions with sun-glitter, rain, and near land. Since only a small number of retrievals are unsuccessful, almost complete global coverage is achieved daily. Any errors in retrieved wind speed, water vapor, cloud liquid water can result in errors in retrieved SST.

Buoy measurements from the Tropical Atmosphere Ocean / Triangle Trans-Ocean Buoy Network (TAO/TRITON) and the Pilot Research Moored Array in the Tropical Atlantic (PIRATA) are used to validate the PMW SSTs. Table 3 shows the mean difference, mean satellite minus buoy SST difference and standard deviation (STD) for each of the buoy arrays. Comparisons with TMI data from 1 January 1998 through 9 June 2005 show that the TAO and PIRATA arrays have very small mean biases, -0.09 C and -0.09 C, and STD of 0.67 C and 0.60 C respectively. Comparisons with AMSR-E data (1 May 2002 through 9 June 2005) show the TAO and PIRATA arrays have very small biases (-0.03 C and -0.01 C) and STD (0.41 C and 0.35 C, respectively).

**Table 3.** Nighttime satellite – buoy SST errors, bias and standard deviation (STD).

Satellite	TOGA TAO/TRITON			PIRATA		
	Collocations	Bias	STD	Collocations	Bias	STD
TMI	84072	-0.09	0.67	11669	-0.09	0.60
AMSR-E	21461	-0.03	0.41	2837	-0.00	0.35

## Sea Surface Salinity

The first measurements of SSS from space will be from the SMOS and Aquarius. SSS is important to ocean circulation, the global hydrological cycle, and climate. Monitoring SSS will provide information on geophysical processes that affect SSS and the global hydrological cycle, such as the sea ice freeze/thaw cycle, evaporation and precipitation over the ocean, and land runoff. The Aquarius mission will attempt to measure SSS with a 150 km spatial resolution and a measurement error of  $< 0.2$  PSS-78 (Practical Salinity Scale of 1978) (Lagerloef *et al.*, 2008).

At 1.4 GHz, retrievals are sufficiently sensitive to SSS to allow for accurate retrieval of SSS. The retrievals depend on the dielectric constant of sea water, the wind-induced sea-surface emissivity and scattering characteristics, atmospheric absorption, particularly that due to rain, and Faraday rotation. Additional contributions from near-land emissions, galactic background radiation reflection, and reflected solar radiation present increased difficulties.

## 6. Erroneous retrievals

### Rain Contamination

The retrievals for SST, wind speed, and vapor must be flagged as bad data in the presence of rain. This is usually done by looking at the simultaneous retrieval of rain rate. Occasionally, sub-pixel rain cells contaminate these retrievals but are not flagged as rain. These can be seen as anomalously warm or cold SSTs or anomalously high wind values, usually only affecting 1-2 pixels in a region where other data nearby has been flagged as rain contaminated. In working with PMW data, area-rain flagging is necessary to remove these anomalously affected cells near rain. Only then can climatological results be trusted.

### Near land emission

Near land, the lobes to the side of the main beam can result in side-lobe contamination. This contamination results in geographic dependent retrieval errors unless the data are flagged as erroneous. This contamination impacts all the geophysical retrievals from PMW radiometers to differing extents depending on the land emission signal at the frequencies included in the various retrieval algorithms. For example, because the 10.7 GHz channels is affected more by land emissions, the land contamination at 10.7 GHz is larger than at 6.9 GHz, resulting in a warm bias and small in-

crease in standard deviation for both TMI and AMSR-E measurements near land, but the effect is larger in the TMI retrievals.

To estimate the side-lobe contamination in the TMI PMW SST retrievals we have compared contemporaneous Visible Infrared Radiometer Scanner (VIRS) IR SST retrievals in coastal regions, using data from January 1998 through December 1998. VIRS is an infrared radiometer carried on the TRMM satellite alongside TMI. VIRS SSTs were determined to have a standard deviation of  $0.7\text{ }^{\circ}\text{C}$  when compared to Reynolds Optimal Interpolated SSTs (Ricciardulli and Wentz, 2004).

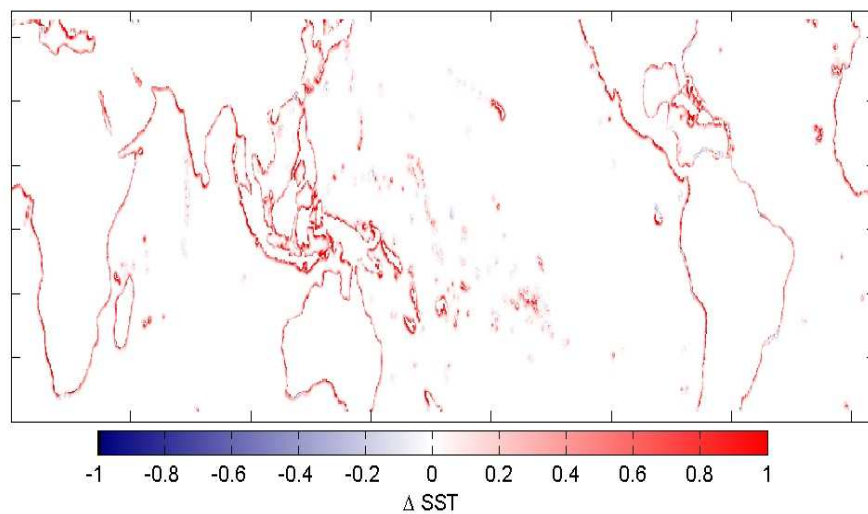


**Fig. 4.** Estimate of bias due to side-lobe contamination near land for 10.7 GHz SST retrievals.

To investigate how the effect of land contamination on the TMI SSTs diminishes away from land, the distance from land for each data point was calculated. The effect of land contamination can be seen in the mean difference, TMI minus VIRS SST (Figure 4). The mean difference away from land is roughly  $0.12\text{ }^{\circ}\text{C}$ , which is approximated by the difference expected between a skin (VIRS) and subskin (TMI) measurement of SST. As the distance to land decreases, the mean difference increases, with a maximum magnitude of  $0.72\text{ K}$ , indicating that the bias due to land contamination is on the order of  $0.6\text{ K}$ . From Figure 5, it is clear that biasing exists mostly for retrievals less than 100 - 150 km from land. These results are specific to the 10.7 GHz SST retrieval from TMI. Although AMSR-E has land contamination also, the impact is less at 6.9 GHz, the primary channel used for AMSR-E SSTs.

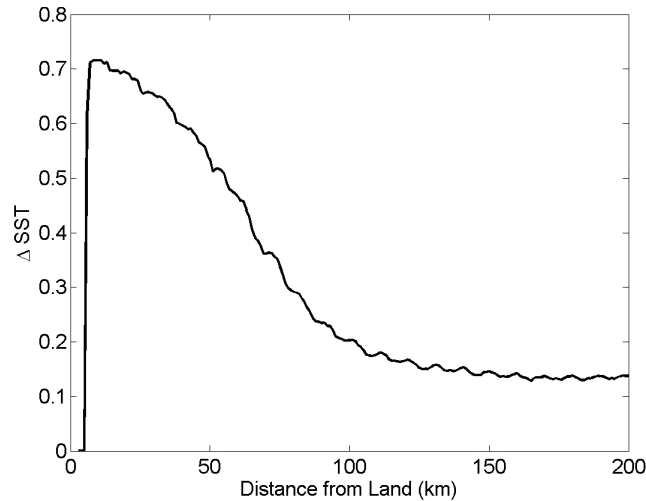


**Fig. 5.** Land contamination bias derived from TMI VIRS comparisons. This global average shows that by removing data within 100 - 150 km of land, sidelobe contamination will be removed.

### Radio Frequency Interference

RFI is arguably the fastest growing source of errors in microwave SSTs and wind speeds. The RFI impact on water vapor, cloud liquid water, and rain rate is less, but growing. RFI errors are largely caused by media broadcasting activities (including television and radio) from commercial satellites in geostationary orbits. Geostationary RFI results when signals broadcast from these communication satellites reflect off the Earth's ocean surface into a PMW instrument's field of view. Ground-based instrumentation in the microwave range is also producing RFI, some sources of which have been identified and characterized. Both these types of anthropogenic RFI are increasing in magnitude and extent. While it is relatively straightforward to identify and flag data affected by large RFI contamination, less-obvious RFI contamination can be difficult to identify. The spatial and temporal nature of the RFI removal must be carefully monitored to avoid spurious trends in climate data records. The addition of new communication satellites, more power, more ground coverage, and the use of more frequencies near PMW instrument measurement bandwidths signify that sources of RFI will continue to change and increase in the future.

The RFI errors resulting from geostationary broadcast sources are primarily dependent on communication broadcast frequency, power and direction, PMW instrument bandwidth, signal glint angle, and ocean surface roughness. The observation bandwidths of PMW instruments are typically

wider than the protected bands allocated for PMW remote sensing. Thus, PMW instruments can receive RFI from legal activity using nearby frequency bands allocated for communication and other commercial uses. AMSR-E and WindSat are the two PMW instruments most affected by RFI, while SSM/I and TMI both appear to be relatively unaffected. This is likely because the lower frequency channels of AMSR-E and WindSat, particularly the 10.7 and 18.7 GHz measurement channels, are sensitive to frequencies used extensively for media broadcasting. WindSat has more significant RFI than AMSR-E due to wider observation bandwidth. Observing more bandwidth tends to yield less noise, but also leads to more interference from frequencies further from the channel's center observation frequency. For example, at 18.7 GHz, WindSat receives interference from DirecTV nationwide broadcast beams. AMSR-E, with narrower bandwidth at 18.7 GHz, does not appear to be significantly affected by nationwide broadcast frequencies, but does receive RFI from DirecTV spot beams, which broadcast at frequencies closer to the center observation frequency of the 18.7 GHz channel.

Power and direction are also important factors affecting RFI. Satellite media broadcasts appear to direct most signal power very carefully to specific markets. Powerful signals can result in large RFI errors within certain regions. To serve smaller but growing geographically dispersed markets, media satellites also broadcast wide, low power beams to cover much larger, less populated regions. These lower power beams induce more subtle RFI effects that can be difficult to detect and remove. Assuming the Earth observation point is within the footprint of a geostationary broadcast, the magnitude of RFI is highly dependent on the glint angle, or how close the observation reflection vector comes to pointing at the RFI source.

RFI induced errors in AMSR-E ocean products were investigated over the entire 7 year mission data set. The effects of the different sources of RFI are listed in Table 4, including which PMW passes are affected and the time period of interference. Because most geostationary broadcast power is directed toward the northern hemisphere, many broadcast beams only reflect into the descending pass AMSR-E field-of-view.

From the start of the AMSR-E mission in 2002, HotBird, which is positioned over 13.0° East longitude, and Astra, located at 19.2° East, have steadily increased RFI in European waters over time. DirecTV-10 at 102.8° West and DirecTV-11 at 99.2° West have produced RFI in American waters since 2007, and Atlantic Bird 4A at 7.2° West has been contributing to Mediterranean Sea RFI since 2009. Also from beginning of mission in 2002, SkyBrazil has directed power toward the southern hemisphere, therefore reflecting into ascending passes of AMSR-E and producing RFI off the coasts of southern Brazil and Argentina.

**Table 4.** Sources of RFI

Source	Region affected	Frequency (GHz)	Effect on data (↓ decreases)	Affected overpass	Period of interference
HotBird	Europe	10.7	↓ SSTs ↑ Winds	Descending	Pre 2002 – present
Astra	Europe	10.7	↓ SSTs ↑ Winds	Descending	Pre 2002 – present
Atl.Bird 4A	Mediterranean	10.7	↓ SSTs ↑ Winds	Descending	Apr 2009 – present
DirecTV-10	USA	18.7	↓ SSTs ↓ Wind ↓ vapor ↑ cloud ↑ rain	Descending	Sep 2007 - present
DirecTV-11	USA	18.7	↓ SSTs ↓ Wind ↓ vapor ↑ cloud ↑ rain	Descending	July 2008 - present
SkyBrazil	SE American Coast	10.7	↓ SSTs ↑ Winds	Ascending	Pre 2002 – present
ground-based	Ascension Island	6.9	↓ SSTs no wind effect	Both	Pre 2002 – present
ground-based	Gulf of Aden	10.7	↓ SSTs ↑ Winds	Both	Mar 2009 - present
ground-based	Coastal Netherlands Coastal Norway	6.9	↑ SSTs no wind effect	Both	2004 - present
ground-based	Mumbai	6.9	↑ SSTs no wind effect	Both	2003 - present

Ground-based RFI sources are also growing stronger and more numerous over time. Unlike the Geostationary RFI, the ground-based RFI affects both ascending and descending swaths, though to different extents. This is likely due to differing levels of RFI activity at the AMSR-E local observation times of 1:30AM or 1:30PM. Although errors caused by these ground-based sources cover fairly small regions, the size and intensity of these RFI effects have been increasing over the years. Ground-based RFI sources can operate intermittently, sometimes even sporadically. The most prominent regions include coastal Netherlands and Norway, coastal Mumbai, the Gulf of Aden through the waters south of Oman, and waters around Ascension Island.

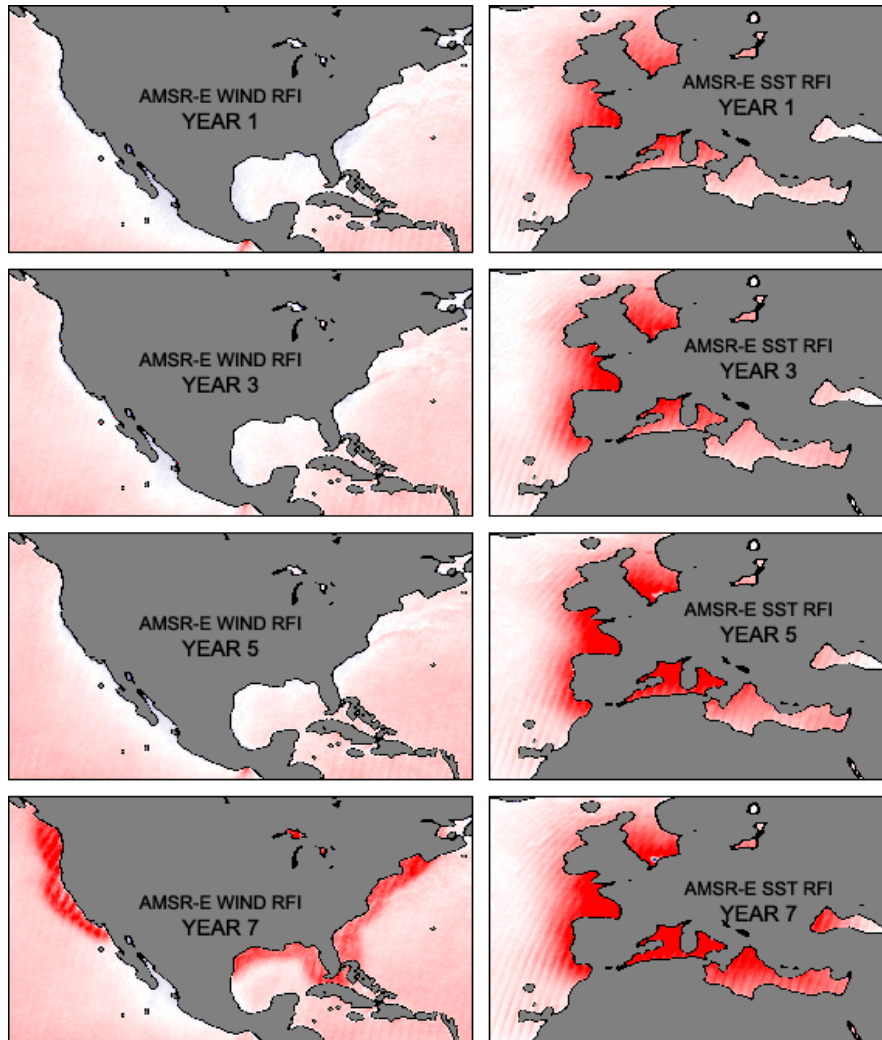


**Fig. 6.** RFI induced wind (left) and SST (right) errors shown in descending pass difference plots for years 1, 3, 5 and 7 of the ASMR-E mission (starting July, 2002, 2004, 2006, 2008) over North America and Europe where the RFI has increased most in coverage and intensity over the years. The striping is caused by the shifting orbital pattern of the most intense geostationary glint angles.

Regions of RFI are located by differencing AMSR-E SSTs derived using all SST channels (6.9 GHz – 36.5 GHz) from those derived without 6.9 GHz (10.7 GHz – 36.5 GHz), as well as by differencing winds derived using all wind channels (10.7 GHz – 36.5 GHz) from those derived without 10.7 GHz (18.7 GHz – 36.5 GHz). An example is shown in Figure 6.

Since most geostationary sources affect the AMSR-E descending passes, this plot shows the wind (North America) and SST (Europe) descending orbit difference maps. The wind RFI around North America caused by DirecTV outlines U.S coastal waters and the Great Lakes (both pictured), with some subtle effects detected as far as Hawaii and possibly the Canary Islands off the coast of Africa (neither shown). The SST RFI around Europe shows consistently increasing extent and intensity over the years.

A ground RFI source off the Netherland coast has concurrently increased power to become more prominent as seen by the small distinctive dot forming over the years. The ground source produces SST errors of opposite sign compared to the geostationary RFI in the region. In this small region, two prominent sources of RFI error tend to cancel each other, potentially complicating detection and removal. The striping visible in Figure 6 is not due to any cross-swath problem with the SSTs or wind speeds, but is due to the glint angle geometry which results in a heavily striped glint angle pattern caused by AMSR-E's ground track repeat pattern every 233 orbits.

Glint angles and broadcast footprints are together highly predictive of potential RFI bias. Therefore, to remove RFI errors from the AMSR-E SST and wind products we calculate the signal glint angles using the longitude of the geostationary orbits. These glint angles, together with analysis of broadcast footprints, are used to remove retrievals with high probability of RFI error.

## 7. Conclusions

PMW retrievals of wind speed, water vapor, cloud liquid water, rain rate, sea ice, and SST have provided key information for research, climate, and operational applications. For research and operational applications, the daily global coverage provided by PMW retrievals are a significant advance over the pre-satellite era which relied on ship and buoy observations. For climate monitoring, the careful inter-calibration of the PMW radiometers and consistent (single algorithm) processing of the entire data set has provided an accurate 22 year time series of PMW retrievals.

## Acknowledgements

The AMSR-E SSTs are from Remote Sensing Systems, processed using the version 5 algorithm, and available at [www.remss.com](http://www.remss.com). This work was funded by the NASA grants NNG04HZ29C, NNG07HW15C, NNH08CC60C, and NNH09CF43C.

## References

- Atlas RM, Hoffman RN, Ardizzone J, Leidner SM, Jusem JC (2009) Development of a new cross-calibrated, multi-platform (CCMP) ocean surface wind product. Paper presented at AMS 13th Conference on Integrated Observing and Assimilation Systems for Atmosphere, Oceans and Land Surface (IOAS-AOLS), Phoenix, AZ, USA
- Bettenhausen MH, Smith CK, Bevilacqua RM, Wang NY, Gaiser PW, Cox SK (2006) A Nonlinear Optimization Algorithm for WindSat Wind Vector Retrievals. *IEEE Trans Geosci Rem Sen* 44(3):597-608
- Bowman KP., Homeyer CR, Stone DG (2009) A Comparison of Oceanic Precipitation Estimates in the Tropics and Subtropics. *Journal of Applied Meteorology and Climatology*, 48:1335-1344
- Cavalieri DJ, Gloersen P, Campbell JW (1984) Determination of Sea Ice Parameters With the Nimbus 7 SMMR. *J Geophys Res* 89:5355-5369
- Cecil DJ, Wingo M (2009) Comparison of TRMM Rain-Rate Retrievals in Tropical Cyclones. *J Meteorol Society Japan* 87A:369-380, doi:10.2151/jmsj.87A.369
- Comiso JC, Cavalieri DJ, Parkinson CL, Gloersen P (1997) Passive Microwave Algorithms for Sea Ice Concentration: a Comparison of Two Techniques. *Rem Sens Environ*, 60(3):357-384
- Comiso JC, Steffen K (2001) Studies of Antarctic Sea Ice Concentrations From Satellite Data and Their Applications. *J Geophys Res* 106(C12):31361-31385
- Gaiser PW, St.Germain KM, Twarog E, Poe G, Purdy W, Richardson D, Grossman W, Jones WL, Spencer D, Golba G, Cleveland J, Choy L, Bevilacqua RM, Chang P (2004) The WindSat Spaceborne Polarimetric Microwave Radiometer: Sensor Description and Early Orbit Performance. *IEEE Trans Geosci Rem Sen* 42(11):2347-2361
- Gentemann CL, Meissner T, Wentz FJ (2009) Accuracy of satellite sea surface temperatures at 7 and 11 GHz. *IEEE Trans Geosci Rem Sen*, in press
- Gloersen P, Cavalieri DJ, Chang ATC, Wilheit TT, Campbell WJ, Johannessen OM, Katsaros KB, Kunzi KF, Ross DB, Staelin D, Windsor EPL, Barath FT, Gudmandsen P, Langham E, Ramseier RO (1984) Summary of Results From the First NIMBUS 7 SMMR Observations. *J Geophys Res* 89:5335-5344

- Han D, Kim ST (1988) Effects of switch leakages upon Nimbus-7 SMMR calibration. 100705, pp. 17, Goddard Space Flight Center, Greenbelt, MD, USA
- Haug GH, Gunther D, Peterson LC, Sigman DM, Hughen KA, Aeschlimann B (2003) Climate and the Collapse of Maya Civilization. *Science* 299:1731-1735
- Held IM, Soden BJ (2006) Robust Responses of the Hydrological Cycle to Global Warming. *J Climate* 19:5686-5699
- Hilburn KA, Wentz FJ (2008) Intercalibrated Passive Microwave Rain Products From the Unified Microwave Ocean Retrieval Algorithm (UMORA). *Journal of Applied Meteorology and Climatology*, 47):778-794
- Hollinger J, Peirce JL, Poe G (1990) SSM/I Instrument Evaluation. *IEEE Trans Geosci Rem Sens* 28(5):781-790
- Kummerow CD, Barnes W, Kozu T, Shieu J, Simpson JJ (1998) The Tropical Rainfall Measuring Mission (TRMM) Sensor Package. *J Atmos Oceanic Technol* 15(3):809-817
- Lagerloef GSE, Colomb FR, Le Vine D, Wentz FJ, Yueh SH, Ruf CS, Lilly J, Gunn Y, Chao A, deCharon A, Feldman G, Swift C (2008) The Aquarius/SAC-D Mission: Designed to Meet the Salinity Remote-Sensing Challenge. *Oceanography* 21:68-81
- Markus T, Cavalieri DJ (2000) An Enhancement of the NASA Team Sea Ice Algorithm. *IEEE Trans Geosci Rem Sens* 38:1387-1398
- Mears CA, Smith DK, Wentz FJ (2001) Comparison of Special Sensor Microwave Imager and Buoy-Measured Wind Speeds From 1987 – 1997. *J Geophys Res* 106(C6):11719-11729
- Meissner T, Smith DK, Wentz FJ (2001) A 10-Year Intercomparison Between Collocated Special Sensor Microwave Imager Oceanic Surface Wind Speed Retrievals and Global Analyses. *J Geophys Res* 106(C6):11731-11742
- Meissner T, Wentz FJ (2009) Wind Vector Retrievals Under Rain With Passive Satellite Microwave Radiometers. *IEEE Trans Geosci Rem Sens* 47(9):3065-3083
- O'Conner T, Kiker GA (2004) Collapse of the Mapungubwe Society: Vulnerability of Pastoralism to Increasing Aridity. *Climatic Change* 66:49-66
- Parkinson CL (2003) Aqua: An Earth-Observing Satellite Mission to Examine Water and Other Climate Variables. *IEEE Trans Geosci Rem Sens* 41(2):173-183
- Petty GW (1994) Physical Retrievals of Over-Ocean Rain Rate From Multichannel Microwave Imagery. Part I: Theoretical Characteristics of Normalized Polarization and Scattering Indices. *Meteorol Atmos Physics* 54:79-99
- Ricciardulli L, Wentz FJ (2004) Uncertainties in Sea Surface Retrievals From Space: Comparison of Microwave and Infrared Observations From TRMM. *J Geophys Res* 109 C12013 doi:10.1029/2003JC002247
- Szczodrak M, Minnett PJ, Gentemann CL (2006) Comprison of AMSR-E retrievals of total water vapor over ocean. paper presented at 2006 Ocean Sciences Meeting, Honolulu, HI, USA

- Trenberth KE, Fasullo J, Smith L (2005) Trends and Variability in Column-Integrated Atmospheric Water Vapor. *Climate Dynamics* 24:741-758
- Wentz FJ (1997) A Well Calibrated Ocean Algorithm for Special Sensor Microwave / Imager. *Journal of Geophysical Research* 102(C4):8703-8718
- Wentz FJ (1998) AMSR Ocean Algorithm. 110398, pp. 66, Remote Sensing Systems, Santa Rosa, CA
- Wentz FJ, Meissner T (2007) AMSR\_E Ocean Algorithms. 051707, pp. 6, Remote Sensing Systems, Santa Rosa, CA, USA
- Wentz FJ, Ricciardulli L, Hilburn KA, Mears CA (2007) How Much More Rain Will Global Warming Bring? *Science* 317:233-235
- Wentz FJ, Schabel MC (2000) Precise Climate Monitoring Using Complementary Satellite Data Sets. *Nature* 403(6768):414-416
- Wentz FJ, Spencer RW (1998) SSM/I Rain Retrievals Within a Unified All-Weather Ocean Algorithm. *J Atmos Sci* 55(9):1613-1627